The Journal of Chemical Physics

RESEARCH ARTICLE | SEPTEMBER 23 2025

Cesium exhibits different mesoscale segregation and ion pairing than lithium, sodium, or potassium in concentrated alkaline aqueous nitrite solutions

Emily T. Nienhuis ; Sebastian T. Mergelsberg ; Trent R. Graham ; Ashley R. Kennedy ; Carolyn I. Pearce ; Jacob G. Reynolds

J. Chem. Phys. 163, 124505 (2025)
https://doi.org/10.1063/5.0286139

The Journal of Chemical Physics ARTICLE pubs.aip.org/aip/jcp

Cesium exhibits different mesoscale segregation and ion pairing than lithium, sodium, or potassium in concentrated alkaline aqueous nitrite solutions

Cite as: J. Chem. Phys. 163, 124505 (2025); doi: 10.1063/5.0286139
Submitted: 18 June 2025 • Accepted: 27 August 2025 •
Published Online: 23 September 2025

Emily T. Nienhuis,[1,a] Sebastian T. Mergelsberg,[1,b] Trent R. Graham,[1,c] Ashley R. Kennedy,[1] Carolyn I. Pearce,[1,2] and Jacob G. Reynolds[3,d]

AFFILIATIONS

[1] Pacific Northwest National Laboratory, Richland, Washington 99354, USA
[2] Department of Crop and Soil Sciences, Washington State University, Pullman, Washington 99164, USA
[3] Central Plateau Cleanup Company, Richland, Washington 99354, USA

[a] emily.nienhuis@pnnl.gov
[b] sebastian.mergelsberg@pnnl.gov
[c] **Author to whom correspondence should be addressed:** trent.graham@pnnl.gov
[d] jacob_g_reynolds@rl.gov

ABSTRACT

Understanding ion pairing in concentrated alkaline electrolytes facilitates the prediction and control of chemical processes in nuclear waste. While sodium is the dominant alkali metal in such systems, cesium often exhibits distinct bulk behavior relative to lighter alkali cations. Aqueous mixtures of cesium hydroxide and sodium nitrite were compared to alkali hydroxide analogs using small-angle x-ray scattering, revealing that cesium disrupts the sodium nitrite electrolyte structure, forming cesium-rich domains. This mesoscale segregation contrasts with the near-ideal mixing observed in other mixed hydroxide–nitrite systems. Raman spectroscopy indicates cesium–nitrite ion pairing, evidenced by vibrational shifts distinct from those associated with sodium. Multinuclear magnetic resonance spectroscopy further supports cesium–nitrite and cesium–hydroxide association, revealing a distinct local environment for nitrite in cesium-containing solutions. Together, these findings show that cesium promotes a unique solution structure dominated by specific ion pairing within segregated domains. This structural organization may influence radical generation pathways in high-ionic-strength alkaline media relevant to nuclear waste processing and management.

I. INTRODUCTION

While thermal and physical properties of many dilute aqueous solutions can be described using electrostatic models, these models inherently fail at high electrolyte concentrations, in which the scarcity of water confines counterions to be proximal to other ions in almost every direction.[1] Stoichiometric considerations illustrate this. Most monovalent ions are coordinated by at least four water molecules, and a kilogram of water contains 55.509 mol of H_2O. Consequently, an electrolyte concentration >6.95 molal for a 1:1 salt (≈13.9 mol of ions kg^{-1} H_2O) will not possess sufficient water molecules to fully hydrate all ions. Thus, many of these highly concentrated solutions form extensive ion networks in which water molecules are chemically confined between ions.

At intermediate concentrations (between 1 and 7 molal), the number of water molecules per ion remains low. Formation of contact ion pairs or larger clusters of ions is then highly dependent on the specific ion identities and their concentrations.[2,3] The cesium (Cs^+) ion is often characterized as "structure-breaking" or

chaotropic, lowering solution viscosity and, in some cases, increasing water self-diffusion rates.[4–6] This phenomenon is now largely understood in terms of its low charge density and its distinct solvation shell structure leading to weaker Cs^+–H_2O interactions compared to H_2O–H_2O interactions.[4,7,8] $CsNO_2$ and $RbNO_2$ can exhibit near-ideal behavior even at very high concentrations under some conditions.[9,10]

The chaotropic behavior of Cs^+ is consistent with Collins's interpretation of Hofmeister effects,[11–14] which distinguish strongly hydrated (kosmotropic) ions from weakly hydrated (chaotropic) ions. Foundational studies show that chaotropic ions contribute to mesoscale segregation and solution structuring. Collins's Law of Matching Water Affinities (LMWA) further clarifies these behaviors, predicting stronger interactions between ions of similar hydration character. The interactions between Cs^+ and NO_2^- observed here are consistent with this framework and supported by reported viscosity B coefficients: $B < 0$ for Cs^+ and -0.024 for NO_2^-.[15] These coefficients reflect molecular-scale dynamics characteristic of chaotropic ions. Although this study emphasizes structural characterization through spectroscopy and diffraction, viscosity data offer a complementary perspective on ion association and mesoscale organization in concentrated electrolytes.

The hydroxide (OH^-) and nitrite (NO_2^-) anions also display complex transport and solubility properties. Hydroxide diffusion under alkaline conditions proceeds through multiple mechanisms, including Grotthuss transport (proton hopping).[16] The diffusion of the nitrite ion also deviates from the Stokes–Einstein relationship.[17,18] Both of these anions can participate in unusual thermodynamic phenomena, such as nitrite increasing the solubility of aluminum hydroxide in alkaline solutions[19] and increasing the solubility of salts with shared ions. The latter of which is inconsistent with the law of mass action.[20,21] Apparent deviations from the law of mass action occur only when chemical equilibrium is interpreted under ideal assumptions. When chemical potentials incorporate non-ideal behavior, the law holds exactly, as demonstrated in prior studies.[22,23] These deviations therefore reflect divergence from ideal approximations in concentrated electrolyte systems.

Our research program focuses on the reactivity and dynamics of ions in intermediate and concentrated solutions, particularly those containing electrolytes, such as nitrite, relevant to alkaline nuclear waste stored at the Hanford Site in Washington State.[24–29] Electrolyte mixtures at high concentrations necessitating the formation of ion networks present distinct structural behavior. Previous work has indicated that Na^+ and nitrite form contact ion pairs in very concentrated $NaNO_2$–H_2O systems[30] and more prominently in NaOH–$NaNO_2$–H_2O systems,[31] although these contacts were not always sufficiently strong to act as distinct thermodynamic ion-pair species.[20,32] These solutions also exhibit both idealized properties, such as linear correlations between diffusion coefficients and water activity, alongside deviations from the law of mass action.[20,32]

The reactivity of ions in these networks under ionizing radiation is also of interest, and photolysis has previously been used to probe subsets of radiolytic pathways. A recent study[33] showed that photolysis product concentrations generally increased with cation size for solutions containing Li^+, Na^+, and K^+, despite their presence being typically regarded as that of a spectator ion. Solutions with Cs^+ did not follow this trend and produced significantly more NO_2· radical. This anomalous behavior of Cs^+ strongly suggests a fundamental difference in its solution chemistry, local ionic environment, or its influence on reactant/product stability relative to smaller alkali cations. Thus, the unique behavior of Cs^+ motivates a closer examination of its solution structure.

The present study investigates the solution structure of aqueous $NaNO_2$ mixtures of alkali hydroxides (LiOH, NaOH, KOH, and CsOH). Our aim was to identify structural distinctions, such as differences in ion aggregation, ion pairing, and solvation, that could rationalize the previously observed spectator ion effect on photolysis. The structure of these solutions was first ascertained with small-angle x-ray scattering (SAXS), followed by additional comparative analysis of $NaNO_2$ in NaOH or CsOH solution using Raman spectroscopy and nuclear magnetic resonance (NMR) spectroscopy. Understanding the distinct solution chemistry of alkali ions provides a basis for developing more refined waste management and remediation strategies of alkaline nuclear waste.

II. EXPERIMENTAL METHODS

A. Solution preparation

All chemicals were used as received. Sodium nitrite was procured from Sigma-Aldrich ($NaNO_2$, 99% purity). Cesium hydroxide (CsOH, 50% w/w, Sigma-Aldrich), sodium hydroxide (NaOH, 50% w/w, Sigma-Aldrich), and potassium hydroxide (KOH, 45% w/w, Sigma-Aldrich) served as alkali hydroxide sources. Deionized (DI) water (18 MΩ cm) was used for all preparations. Concentrated stock solutions of $NaNO_2$ were prepared by dissolving solids in DI water in volumetric flasks. Multicomponent electrolyte solutions consisted of a fixed concentration of 1.0M $NaNO_2$ combined with varying concentrations of a specific alkali hydroxide (MOH, where M = Cs, K, or Na). These multicomponent solutions were prepared by the volumetric addition of $NaNO_2$ stock solution and the appropriate MOH stock solution followed by dilution with DI water in volumetric glassware. All reagent handling and solution preparation steps, for both stock solutions and the final mixed solution series, were conducted within a N_2-atmosphere glovebox.

B. Small-angle x-ray scattering

SAXS data were acquired at beamline 12-ID-C of the APS using a constant incident photon energy of 20 keV ($\lambda = 0.6199$ Å) to measure samples in transmission through a 1.5 mm ID silica capillary (Charles Supper SiO_2 capillaries, 10 μm wall thickness). The beam center and detector configuration were calibrated using a silver behenate standard. For each sample, data were captured for 30 exposures of 1 s each at a sample-to-detector distance of 2.188 m from $q = 0.008$ to 1 $Å^{-1}$. The water and solutions were pumped into the capillary using an automatic sampler and constantly agitated in the capillary to avoid heating or settling of the sample. All data processing was completed using Irena 2.72[34] in IgorPro 9.02 (WaveMetrics, Inc., Lake Oswego, OR, USA). Data were normalized using in-line photodiodes and scaled by measuring water under identical conditions to the samples. Samples were then averaged for each composition. The averaged background scattering patterns of the

silica capillary were then subtracted from all samples. All data were fit using the unified scattering model[35–37] and one peak function to account for the pre-peak scattering.

C. Raman spectroscopy

Raman spectroscopy was performed on a Horiba LabRAM HR spectrometer with a Nikon Ti-E inverted microscope. A 632.81 nm continuous laser light source was focused through a 40× microscope objective. Spectra were collected between 100 and 4000 cm^{-1} and averaged over ten scans with 30 s exposures per spectral region. The background in the region of interest was approximated by a spline function, followed by fitting Lorentzian line shapes to the data. The fitting parameters were obtained by minimizing the sum of the squared residuals between the background corrected experimental data and the model using MS Excel's integrated Solver tool with a gradient descent algorithm.

D. Multinuclear nuclear magnetic resonance spectroscopy

Nuclear magnetic resonance (NMR) spectra were acquired at a field strength of 11.7467 T. For ^{1}H, ^{15}N, and ^{23}Na, spectra were recorded on an Agilent/Varian spectrometer equipped with a 5 mm broadband probe. For ^{17}O and ^{133}Cs, spectra were recorded on a Bruker spectrometer, also utilizing a 5 mm broadband probe. At 11.7467 T, the Larmor frequencies are ~500.13 MHz for ^{1}H, 50.69 MHz for ^{15}N, 67.80 MHz for ^{17}O, 132.33 MHz for ^{23}Na, and 65.62 MHz for ^{133}Cs.

III. RESULTS AND DISCUSSION

A. Small-angle x-ray scattering data

Small-angle x-ray scattering (SAXS) patterns of aqueous solutions are sensitive to the (A) water scattering peak that describes the average O–O distance in water, (B) peaks arising from cation–cation and cation–anion ordering, and (C) local fluctuations in electron density due to ion pair or cluster formation beyond hydration shells of single ions. The features observed as (B) and (C) may have complex origins in electrolyte solutions. Dissolution of organic liquids and some salts in water produces nano- or microemulsions, which refer to randomly distributed spatial heterogeneities of electron density. These "pockets" of solute-rich (or solvent-rich) domains produce enough electron contrast to scatter, producing feature (C) corresponding to the coherence length of these domains. At higher solute concentrations, these randomly distributed "pockets" are close to each other consistently enough to produce peaks (B) that correspond to the so-called repeat distances. Underlying the peaks (B) and local fluctuations in electron density (C) is also a measurement of the average electron density of the solution, which determines the scattering intensity outside the main features.

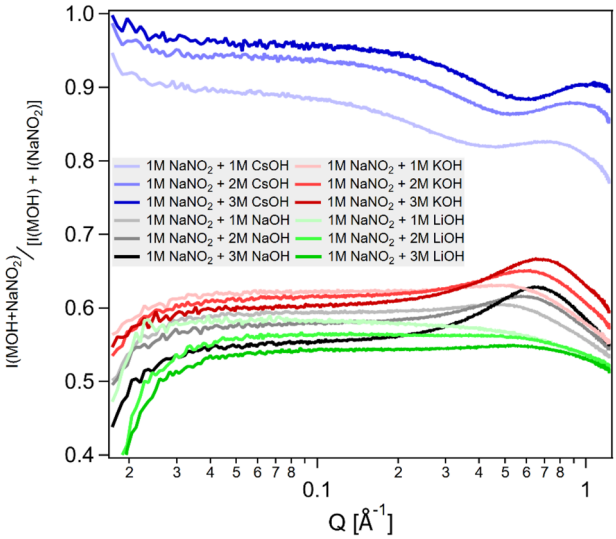

FIG. 2. SAXS signal of mixed solutions divided by the sum of the components.

In the pure NaOH and $NaNO_2$ systems, only feature (C) is observed, indicating the presence of clusters with very little coherence (Fig. 1). As shown in the supplementary material, the scattering profiles of LiOH and KOH are much like the scattering profiles of NaOH. In the mixed hydroxide–nitrate system, we divided the mixed SAXS signal by the sum of the SAXS signal for each component (Fig. 2). The resulting profiles indicate that the average scattering intensity for most alkali systems is close to the average intensity of the two components (0.5), which decreases as a function of hydroxide concentration. The exception is CsOH, which is closer to an additive intensity of the two components that increases as a

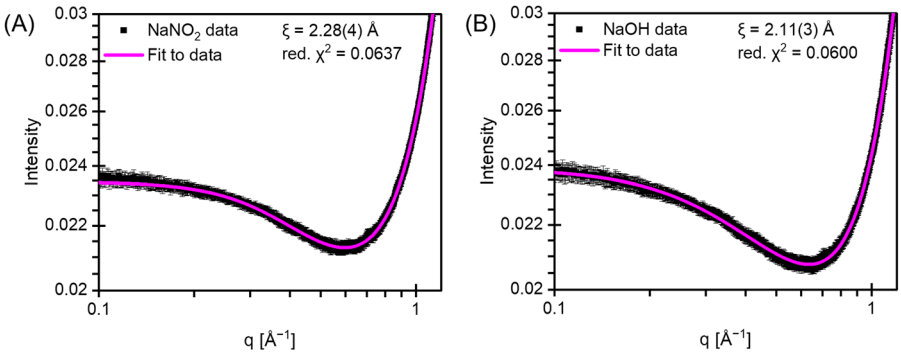

FIG. 1. SAXS data of the (A) $NaNO_2$ and (B) NaOH solutions. The data are fit with a coherence length (ξ) model often used for polymer scattering in solution.[38] At 1M concentration, both solutions exhibit some coherence length features with similar length scales of 2–2.5 Å.

function of hydroxide intensity. This empirical measure is a qualitative indicator of relative solution ordering in the mixed system. While SAXS intensity values are not mathematically additive due to their dependence on the squared modulus of the scattering amplitude, our normalization approach empirically evaluates deviations from randomness in mixing behavior.

In addition to the differences in the average background value, the signal at higher q ($q > 0.3$ Å^{-1}) also shows the emergence of peaks in all systems except for CsOH. These peaks are examples of feature (B) above and represent the repeat distances of the coherent clusters in solution. As the total ion concentration increases, these peaks move to higher q values, consistent with shorter distances between domains. The Cs system is a clear outlier in this region of the SAXS pattern as well. There is no clear emergence of a peak, and we observe emergence of local density fluctuation features (C) at $q \approx 0.2$ Å^{-1} instead. This suggests that the addition of $NaNO_2$ to CsOH causes the formation of additional short-range clusters not present in either pure electrolyte solution.

The limited extent of mixing between CsOH and $NaNO_2$ in solution can also be illustrated quantitatively by fitting the SAXS data. In the case of pure CsOH solutions, the main SAXS signal is a cation–cation peak that measures mean Cs–Cs distances of 8.8 Å at 1M concentration (Fig. 3). The predicted cation–cation distance of a one molar solution is 11.8 Å, assuming random distribution. This implies that the cations are, on average, closer together than one would expect from first principles. The cation–cation distance decreases as a function of concentration and, upon addition of $NaNO_2$, is approximately a function of concentration cubed. The electron density background, I_0, increases as a function of concentration, showing a similar cubed dependence. SAXS data thus suggest that the solution structure of the CsOH system is likely preserved at all concentrations. The two trends are similar. A higher concentration or the addition of $NaNO_2$ simply increases the number density, without significantly affecting the relative distribution of ions.

The observed concentration-cubed dependence of cation–cation distances in CsOH–$NaNO_2$ systems is consistent with the structuring behavior reported for highly concentrated ionic systems. Perkin and coauthors have noted apparent Debye length anomalies in ionic liquids that exhibit high salt decay lengths deviating from classical screening models.[39–41] This "re-entrant" behavior, also observed in high-concentration polyelectrolyte solutions,[42] highlights emergent mesoscale effects driven by concentration scaling in non-ideal systems. The effect is also highly dependent on the charge of the ions.[43]

Insights from the concentration-cubed dependence reported here may complement these broader observations of high salt decay lengths by suggesting similar deviations from bulk screening theories. While the present study focuses on structural measurements from spectroscopy and diffraction techniques, the connection between concentration-dependent ion distances and decay length anomalies provides a compelling framework for further exploration of transport and electrostatic properties in these systems.

The CsOH–$NaNO_2$–H_2O system was the outlier among the alkali hydroxides across the studied series because SAXS data did not show signs of a truly mixed solution, implying largely separate Cs-rich and Na-rich domains. The high electron density of the background suggests that the Cs-rich domains accumulate nitrite anions. The other alkali hydroxide–sodium nitrite systems all showed near-ideal mixing, whereas the Cs^+ system did not. This pronounced difference in medium-range (5–15 Å) structuring observed for the Cs^+ system raises questions about the ion-pairing and the molecular-level interactions underpinning the medium-range SAXS observations. The following Raman and multinuclear NMR spectroscopic analyses focus on comparing the CsOH–$NaNO_2$–H_2O system with the NaOH–$NaNO_2$–H_2O system. The latter ternary system is more compositionally relevant to the Hanford and Savannah River Site nuclear wastes.[44]

B. Raman spectroscopy

Raman spectroscopy probes the local chemical environment of NO_2^- through its characteristic vibrational modes.[45] These include the symmetric deformation (ν_2) near 817 cm^{-1}, the antisymmetric stretch (ν_3) near 1242 cm^{-1}, and the symmetric stretch (ν_1) near 1331 cm^{-1}, as shown in Fig. 4. Example spectral fits are provided in the supplementary material. Analysis of these

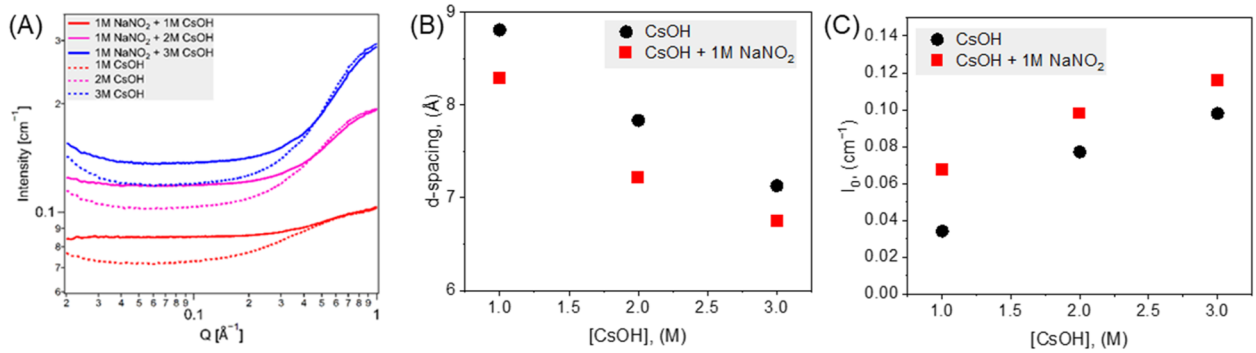

FIG. 3. SAXS data of CsOH solutions. (a) Background-subtracted data show differences in the background and shifts in the scattering peak. (b) Differences in the fit peak position as a function of [CsOH], displayed as d-spacing, where $d = \frac{2\pi}{Q_{peak}}$. (c) Differences in the fit background intensity, I_0, as a function of [CsOH].

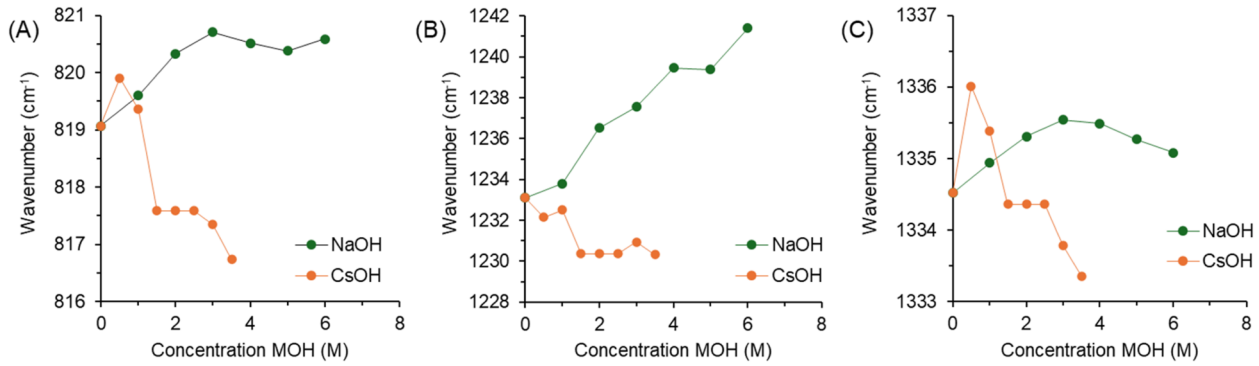

FIG. 4. Raman spectroscopy line shape deconvolutions of nitrite as a function of concentration of sodium hydroxide or cesium hydroxide. The peak position is shown of the band assigned to the (a) symmetric deformation, (b) antisymmetric stretch, and (c) symmetric stretch.

bands in mixed hydroxide–$NaNO_2$ solutions reveals distinct cation-dependent behavior. In 1M $NaNO_2$ solutions, all three nitrite bands shift systematically to higher wavenumbers with increasing NaOH concentration. In contrast, CsOH addition induces shifts of these same bands to lower wavenumbers (Fig. 4).

The frequency shifts observed in the Raman spectra (Fig. 4) reflect changes in nitrite vibrational modes driven by evolving intermolecular forces and solvation environments. These shifts arise from a combination of factors, including Cs^+–NO_2^- ion pairing, changes in solvation dynamics, and mesoscale structuring at higher concentrations. The direction of the shift depends on the vibrational mode and the nature of the perturbation. Stronger cation–anion interactions or rigid solvation shells can produce upshifts, while clustering or dynamic disorder may cause downshifts. Rather than indicating discrete, resolvable ion-pair species, we suggest that these shifts reflect a distribution of local environments. The resulting band asymmetry at high concentrations is best understood as arising from a continuum of overlapping solvation states that evolve with composition.

These divergent frequency shifts of the cesium hydroxide and sodium hydroxide systems provide direct spectroscopic evidence for differing predominant cation–nitrite interactions. The shift to higher wavenumbers with increasing Na^+ concentration, while not producing a new, resolved ion-pair band as sometimes observed for divalent cations,[46,47] indicates a progressive change in the NO_2^- environment consistent with significant Na^+–NO_2^- association and the polarizing effect of Na^+. Conversely, the shift to lower wavenumbers upon CsOH addition aligns with the established trends for ion pairing between NO_2^- and larger alkali cations, such as Cs^+.[48,49] This suggests that Cs^+ ions effectively compete with Na^+ for proximity to NO_2^-, leading to a substantial population of Cs^+–NO_2^- associations, a conclusion consistent with SAXS evidence for Cs-rich domains incorporating nitrite.

In prior studies of $NaNO_2$ solutions,[31] the absence of a new resolved ν_2 band was interpreted as evidence for weak Na^+–NO_2^- ion pairing. While our data for Na^+ and Cs^+ solutions also lack such a new band, the observed systematic shift to higher frequencies for Na^+–NO_2^- interactions and a shift to lower frequencies for Cs^+–NO_2^- agree with the established trends for alkali nitrite ion pairs.[31] Thus, our study highlights that systematic shifts in existing Raman bands can serve as reliable markers for these specific cation–nitrite interactions, with the direction of the shift distinguishing between Na^+ and Cs^+.

Fourier transform infrared (FTIR) spectra were collected to complement the vibrational analysis. The nitrite band near 1235 cm^{-1} exhibited trends consistent with the Raman data, showing a progressive upshift in NaOH solutions and a slight downshift in CsOH. These spectra are provided in the supplementary material. Overall, the SAXS, Raman, and FTIR data suggest distinct cation-specific interactions with NO_2^- and significant Cs^+–NO_2^- association. To further characterize solvation, ion pairing, and the overall solution structure, multinuclear NMR spectroscopy was performed on the ^{17}O, ^{1}H, ^{23}Na, ^{133}Cs, and ^{15}N nuclei.

C. Multinuclear NMR spectroscopy

Multinuclear NMR spectroscopy enables ensemble characterization of H_2O and OH^- environments, as well as selective measurement of the cations (Na^+ and Cs^+) and the nitrite anion. The ^{17}O NMR signal for H_2O/OH^- and the ^{1}H NMR signal for bulk water protons revealed electrolyte-induced changes in the solvent environment. As shown in Fig. 5, increasing CsOH or NaOH concentration caused the ^{17}O H_2O/OH^- chemical shift to increase (downfield) and its linewidth to broaden (e.g., for 3M CsOH, 0–9.84 ppm; width 64.5–75.1 Hz; for 3M NaOH, 0–5.08 ppm; width 68.1–93.5 Hz, in $NaNO_2$-free solutions). These changes are characteristic of increasing OH^- contribution.[50,51] Solvent perturbation is further intensified by reduced water availability at high solute concentrations. A stoichiometric mass balance, assuming primary hydration numbers (Na^+ = 6, Cs^+ = 8, OH^- = 4, and NO_2^- = 6)[52] and no initial ion pairing, predicts complete depletion of free water in 1M $NaNO_2$ + 3.0M CsOH. While simplified, this model highlights the extent of solvent stress under these conditions.

This water scarcity likely amplifies the observed spectral changes. Notably, at 1M hydroxide (without $NaNO_2$), CsOH

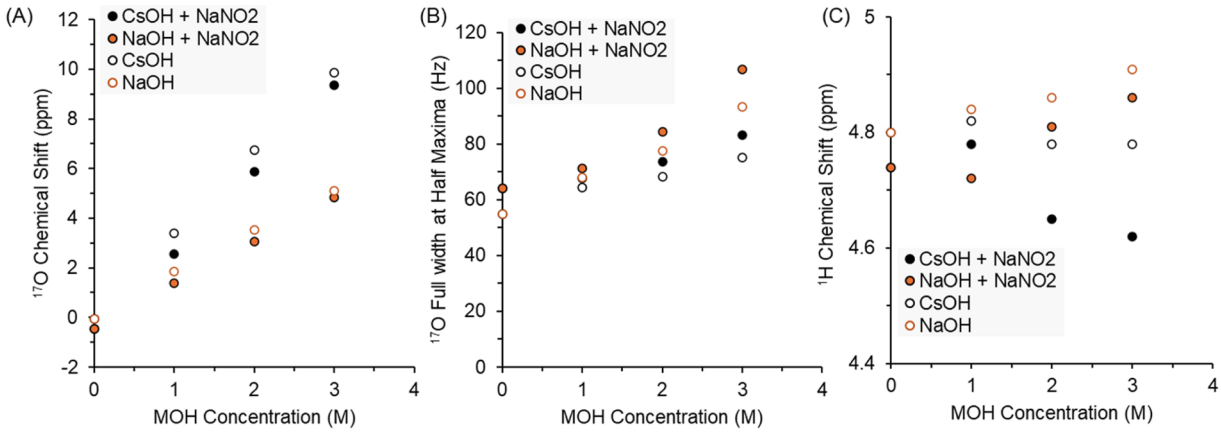

FIG. 5. (a) ^{17}O peak position and (b) ^{17}O full width at half maxima. (c) The peak position of the ^{1}H resonance is shown. The peak positions are externally referenced to a solution of deionized water.

induced a larger downfield shift in the ^{17}O H_2O/OH^- signal (3.41 ppm) than NaOH (1.87 ppm). This difference may reflect the weaker hydration of Cs^+,[4,7] allowing its solvation environment to adjust more readily under stress and thereby altering the average OH^-/H_2O environment differently than Na^+. The presence of 1M $NaNO_2$ slightly modulated these ^{17}O shifts, generally shifting them upfield. Complementary ^{1}H NMR measurements showed divergent trends: increasing CsOH caused a slight upfield shift (e.g., 4.78–4.62 ppm from 1M to 3M CsOH), whereas increasing NaOH led to a slight downfield shift (e.g., 4.74–4.85 ppm from 0M to 3M NaOH), consistent with the concentration-dependent behavior reported previously.[51,53] The ^{1}H chemical shift at concentrations of 1M NaOH + 1M $NaNO_2$ and 1M CsOH + 1M $NaNO_2$ deviated from the linear interpolation of the proximal data points. We speculate that this deviation is due to having equivalent amounts of OH^- and NO_2^- for the case of the NaOH + $NaNO_2$ system and equal amounts of Cs and Na for the CsOH + $NaNO_2$ system, although the trends of ^{1}H are generally small and, as a spin-half nucleus, would be highly sensitive to magnetic field inhomogeneity. Likewise, given the sensitivity of the spin-half nucleus to magnetic field inhomogeneity, the full width half maximum (FWHM) of the ^{1}H resonances is not reported. Despite this, the overall trends in ^{1}H NMR shifts, although influenced by multiple factors, primarily reflect global hydrogen bonding and highlight differences in the hydration characteristics of Na^+ and Cs^+ ions within aqueous electrolytes.

NMR spectroscopy of ^{23}Na and ^{133}Cs nuclei then assessed the local environment of cations. For ^{23}Na, increasing total Na^+ (via NaOH) resulted in downfield shifts and increased linewidths (e.g., 0.33–0.87 ppm for 1–3M NaOH; Fig. 6). More significantly, in CsOH–$NaNO_2$–H_2O, increasing CsOH also shifted the ^{23}Na signal (from $NaNO_2$) downfield (0.25–0.79 ppm for 1M–3M CsOH in 1M $NaNO_2$) and broadened its linewidth (13.05–16.74 Hz). This deshielding and broadening of Na^+ by CsOH indicates substantial alteration of the Na^+ environment, likely due to interaction

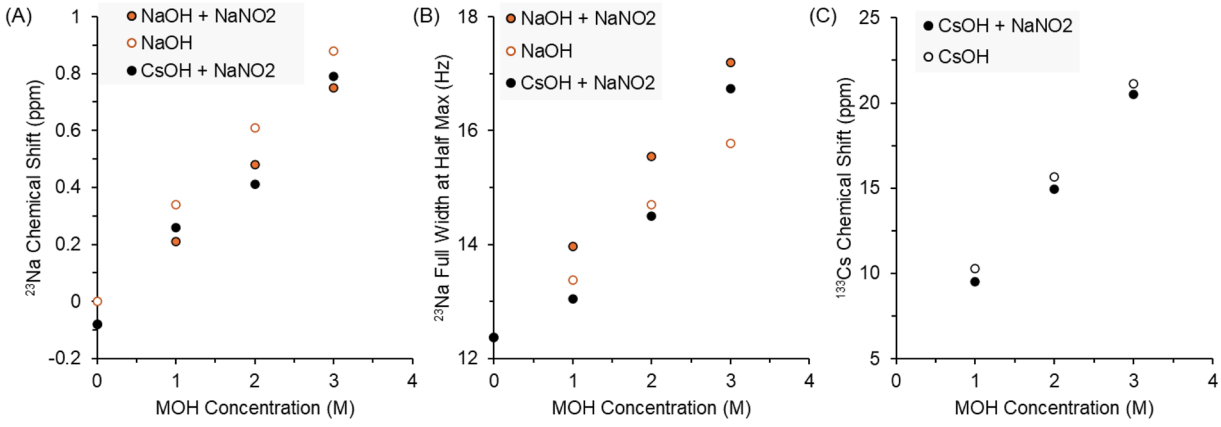

FIG. 6. (a) ^{23}Na peak position and (b) ^{23}Na full width at half maxima. (c) The peak position of the ^{133}Cs resonance is shown. The peak positions are externally referenced to ~1M ^{15}N-enriched $NaNO_2$ in H_2O and a solution of 1 m $CsNO_3$ in H_2O.

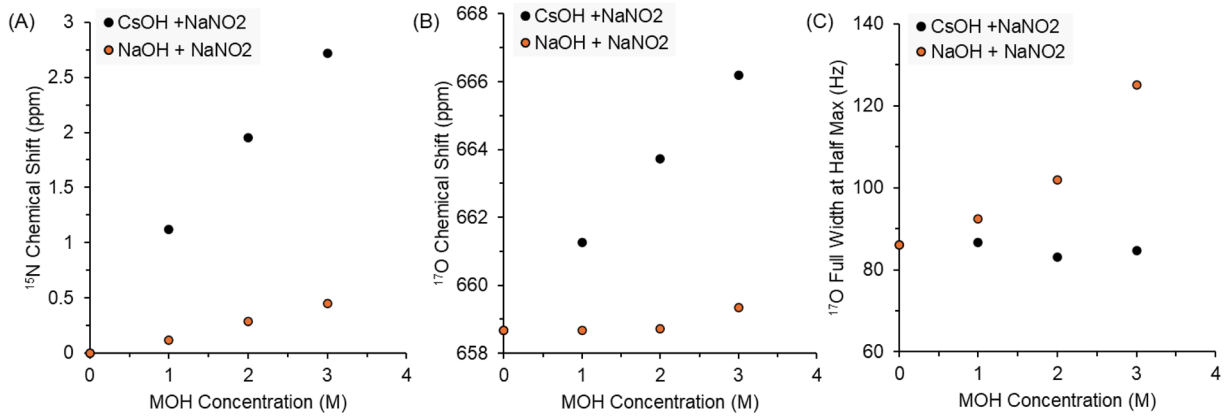

FIG. 7. (a) ^{15}N and (b) ^{17}O NMR peak position of nitrite. (c) The ^{17}O full width at half of the nitrite resonance is shown. The peak positions are externally referenced to ~1M ^{15}N-enriched $NaNO_2$ in H_2O.

with hydrated OH^- or competition for NO_2^-. ^{133}Cs NMR spectra revealed a pronounced ~10 ppm downfield shift as CsOH concentration increased (0M–3M), indicating significant changes in Cs^+ electronic environment due to increased ion pairing (Cs^+–OH^-) and altered solvation (Fig. 6). While 1M $NaNO_2$ offset ^{133}Cs shifts by a few ppm, the slope vs CsOH concentration remained similar, suggesting that $NaNO_2$ subtly influences the average Cs^+ environment, but CsOH concentration drives the primary ^{133}Cs shift.

^{15}N and ^{17}O NMR of NO_2^- probed local interactions of nitrite, as shown in Fig. 7. Increasing CsOH or NaOH in 1M $NaNO_2$ solutions led to ^{15}N (CsOH: 1.11–2.71 ppm; NaOH: 0.0045–0.44 ppm) and ^{17}O–NO_2^- (CsOH: 661.25–666.18 ppm; NaOH: 658.68–659.35 ppm) downfield shifts (deshielding), consistent with the Raman evidence of cation–NO_2^- association. The deshielding was more pronounced with CsOH. A striking difference occurred in ^{17}O–NO_2^- linewidths. Increasing NaOH significantly broadened the peak (86.0–125.0 Hz from 0M to 3M NaOH), whereas CsOH caused only slight fluctuations (e.g., 86.7–84.6 Hz from 1M to 3M CsOH; Fig. 7). The NaOH-induced broadening of the ^{17}O resonance is interpreted to reflect Na^+ interactions generating a more asymmetric electric field gradient, in addition to contributions from viscosity. The relatively stable ^{17}O–NO_2^- linewidth with CsOH—despite evidence of Cs^+–NO_2^- association—may indicate that these interactions occur in a more symmetric local environment, potentially consistent with NO_2^- incorporation into uniform Cs^+-dominated domains, as also suggested by SAXS and Raman analyses. Although empirical models, such as quadratic fits, can capture the observed trends, they may not reflect the underlying physical mechanisms. The relatively stable linewidths in CsOH solutions likely reflect a symmetric, uniform environment for NO_2^- within Cs^+-dominated domains. In contrast, the pronounced broadening in NaOH solutions may arise from asymmetric electric field gradients and viscosity effects. Accurately modeling this behavior will require further investigation of mesoscale structuring and ion clustering, which remains a valuable direction for future work.

Key NMR observations include more pronounced H_2O/OH^- deshielding with CsOH, significant ^{133}Cs chemical shifts, CsOH-induced perturbations to the ^{23}Na environment, and distinct effects on ^{17}O–NO_2^- linewidths. Collectively, these findings demonstrate that Cs^+ ions actively restructure the solution. This restructuring involves associations with NO_2^- and OH^-, consistent with the medium-range heterogeneity observed using SAXS and the specific Cs^+–NO_2^- interactions identified by Raman spectroscopy.

IV. CONCLUSIONS

The collective evidence from SAXS, Raman, and multinuclear NMR spectroscopy suggests unique structural organization in aqueous solutions containing CsOH, particularly with $NaNO_2$, distinguishing them from systems with lighter alkali cations. SAXS revealed mesoscale segregation into Cs-rich domains, indicative of limited mixing, while Raman spectroscopy confirmed preferential Cs^+–NO_2^- association characterized by distinct vibrational shifts. Multinuclear NMR further substantiated these findings, highlighting significant Cs^+-induced perturbations to the solvent and ionic environments, strong Cs^+–NO_2^-/OH^- pairing, and a notably different local environment for the ^{17}O NMR resonance of nitrite associated with Cs^+ relative to Na^+. This convergence of multi-technique data reveals a fundamentally distinct solution architecture driven by Cs^+ ions and offers a rationale for the increased NO_2· radical production observed in cesium-containing systems.[33] The preferential association of NO_2^- within Cs-rich domains, coupled with the direct electronic influence of the large, polarizable Cs^+ ion, is thereby linked to the intrinsic reactivity of nitrite, potentially lowering activation barriers for radical formation or modifying reaction pathways. Furthermore, the unique microenvironment within these Cs-rich domains, characterized by specific solvation, water scarcity effects, and distinct ion dynamics, may enhance radical escape by modifying cage effects or stabilizing radical intermediates. Future work may involve constructing ternary phase diagrams for CsOH–$NaNO_2$–water systems to identify conditions under which mesoscale segregation arises, analogous to surfactant-driven self-assembly in microemulsions.

Conductivity measurements could offer complementary insights into transport properties, potentially distinguishing Cs^+-dominated solutions from Na^+-dominated solutions. Together with the spectroscopic and structural findings reported here, these results provide a robust foundation for understanding the unique behavior of Cs^+ in complex electrolytes and its ion-specific impacts on radiolytic processes in systems relevant to nuclear waste.

SUPPLEMENTARY MATERIAL

See the supplementary material for details on small-angle x-ray scattering (SAXS) patterns of KOH and LiOH solutions, both with and without $NaNO_2$ (Fig. S1); Raman spectral fits of cesium hydroxide + sodium nitrite solutions annotated with sample composition, peak position, full width at half maximum, and relative signal area (Fig. S2); Raman spectral fits of sodium hydroxide + sodium nitrite solutions with the same annotations (Fig. S3); Lorentzian line shape parameters from Raman spectroscopy (Table S1–S4); and Fourier transform infrared (FTIR) spectroscopy attenuated total reflectance (ATR) spectra of aqueous $NaNO_2$ solutions with varying NaOH and CsOH concentrations, including acquisition parameters, key vibrational features, and trends in nitrite band shifts (Fig. S4).

ACKNOWLEDGMENTS

This research was supported by IDREAM (Ion Dynamics in Radioactive Environments and Materials), an Energy Frontier Research Center funded by the U.S. Department of Energy (DOE), Office of Science, Basic Energy Science (Grant No. FWP 68932). A graduate fellow, Ashley Kennedy's work was supported by the Department of Energy Office of Environmental Management Minority Serving Institutions Partnership Program (EM MSIPP). Raman spectroscopy was performed using facilities at the Environmental Molecular Science Laboratory (Grant No. 436923.9), a DOE Office of Science User Facility sponsored by the Office of Biological and Environmental Research at Pacific Northwest National Laboratory (PNNL). PNNL is a multiprogram national laboratory operated for DOE by Battelle Memorial Institute operating under Contract No. DE AC05-76RL0-1830. This research used resources of the Advanced Photon Source, a U.S. Department of Energy (DOE) Office of Science user facility operated for the DOE Office of Science by Argonne National Laboratory under Contract No. DE-AC02-06CH11357.

AUTHOR DECLARATIONS

Conflict of Interest

The authors have no conflicts to disclose.

Author Contributions

Emily T. Nienhuis: Conceptualization (equal); Investigation (equal); Methodology (equal); Writing – original draft (equal). **Sebastian T. Mergelsberg**: Investigation (equal); Methodology (equal); Writing – original draft (equal); Writing – review & editing (equal). **Trent R. Graham**: Data curation (equal); Formal analysis (equal); Methodology (equal); Visualization (equal); Writing – original draft (equal); Writing – review & editing (equal). **Ashley R. Kennedy**: Data curation (equal); Methodology (equal); Visualization (equal); Writing – review & editing (equal). **Carolyn I. Pearce**: Funding acquisition (equal); Project administration (equal); Resources (equal); Supervision (equal). **Jacob G. Reynolds**: Investigation (equal); Supervision (equal); Writing – original draft (equal); Writing – review & editing (equal).

DATA AVAILABILITY

The data that support the findings of this study are available from the corresponding author upon reasonable request.

REFERENCES

[1] Y. Marcus, Chem. Rev. **109**, 1346–1370 (2009).
[2] Y. Marcus and G. Hefter, Chem. Rev. **106**, 4585–4621 (2006).
[3] N. F. A. van der Vegt, K. Haldrup, S. Roke, J. Zheng, M. Lund, and H. J. Bakker, Chem. Rev. **116**, 7626–7641 (2016).
[4] C. F. Schwenk, T. S. Hofer, and B. M. Rode, J. Phys. Chem. A **108**, 1509–1514 (2004).
[5] T. R. Merton, J. Chem. Soc., Trans. **97**, 2454–2463 (1910).
[6] D. W. McCall and D. C. Douglass, J. Phys. Chem. **69**, 2001–2011 (1965).
[7] J. Mähler and I. Persson, Inorg. Chem. **51**, 425–438 (2012).
[8] J. G. Reynolds, J. Mol. Liq. **395**, 123824 (2024).
[9] J. G. Reynolds, Chem. Phys. Lett. **749**, 137439 (2020).
[10] A. A. Zavitsas, Chem. Phys. Lett. **759**, 137941 (2020).
[11] K. D. Collins, Q. Rev. Biophys. **52**, e11 (2019).
[12] K. D. Collins, G. W. Neilson, and J. E. Enderby, Biophys. Chem. **128**, 95–104 (2007).
[13] K. D. Collins and M. W. Washabaugh, Q. Rev. Biophys. **18**, 323–422 (1985).
[14] K. D. Collins, Biophys. J. **72**, 65–76 (1997).
[15] H. D. B. Jenkins and Y. Marcus, Chem. Rev. **95**, 2695–2724 (1995).
[16] R. A. Noulty and D. G. Leaist, J. Solution Chem. **13**, 767–778 (1984).
[17] P. Banerjee, S. Yashonath, and B. Bagchi, J. Chem. Phys. **146**, 164502 (2017).
[18] T. R. Graham, Y. Wei, E. D. Walter, E. T. Nienhuis, J. Chun, G. K. Schenter, K. M. Rosso, C. I. Pearce, and A. E. Clark, Chem. Commun. **59**, 14407–14410 (2023).
[19] M. Dembowski, M. M. Snyder, C. H. Delegard, J. G. Reynolds, T. R. Graham, H.-W. Wang, I. I. Leavy, S. R. Baum, O. Qafoku, M. S. Fountain, K. M. Rosso, S. B. Clark, and C. I. Pearce, Phys. Chem. Chem. Phys. **22**, 4368–4378 (2020).
[20] J. G. Reynolds, M. Dembowski, T. R. Graham, and C. Pearce, Fluid Phase Equilib. **532**, 112922 (2021).
[21] J. G. Reynolds, E. T. Nienhuis, S. T. Mergelsberg, C. I. Pearce, and K. M. Rosso, J. Mol. Liq. **377**, 121470 (2023).
[22] M. E. Fisher and D. M. Zuckerman, J. Chem. Phys. **109**, 7961–7981 (1998).
[23] M. J. Uline and D. S. Corti, J. Chem. Educ. **83**, 138 (2006).
[24] T. R. Graham, A. R. Kennedy, J. Morton, J. G. Reynolds, and C. I. Pearce, Commun. Chem. **8**, 180 (2025).
[25] J. G. Reynolds, J. K. McCoskey, and D. L. Herting, Ind. Eng. Chem. Res. **55**, 5465–5473 (2016).
[26] T. R. Graham, M. Dembowski, E. Martinez-Baez, X. Zhang, N. R. Jaegers, J. Hu, M. S. Gruszkiewicz, H.-W. Wang, A. G. Stack, M. E. Bowden, C. H. Delegard, G. K. Schenter, A. E. Clark, S. B. Clark, A. R. Felmy, K. M. Rosso, and C. I. Pearce, Inorg. Chem. **57**, 11864–11873 (2018).
[27] H.-W. Wang, E. T. Nienhuis, T. R. Graham, M. Pouvreau, J. G. Reynolds, M. Bowden, G. K. Schenter, J. J. De Yoreo, K. M. Rosso, and C. I. Pearce, Commun. Chem. **7**, 199 (2024).
[28] R. A. Peterson, E. C. Buck, J. Chun, R. C. Daniel, D. L. Herting, E. S. Ilton, G. J. Lumetta, and S. B. Clark, Environ. Sci. Technol. **52**, 381–396 (2018).

[29] A. J. Krzysko, T. R. Graham, M. Dembowski, C. Beck, X. Zhang, K. M. Rosso, S. B. Clark, and C. I. Pearce, ACS Earth Space Chem. **6**, 999–1010 (2022).
[30] Y. Wei, E. T. Nienhuis, S. T. Mergelsberg, T. R. Graham, Q. Guo, G. K. Schenter, C. I. Pearce, and A. E. Clark, Chem. Commun. **59**, 10400–10403 (2023).
[31] T. R. Graham, M. Dembowski, H.-W. Wang, S. T. Mergelsberg, E. T. Nienhuis, J. G. Reynolds, C. H. Delegard, Y. Wei, M. Snyder, I. I. Leavy, S. R. Baum, M. S. Fountain, S. B. Clark, K. M. Rosso, and C. I. Pearce, Phys. Chem. Chem. Phys. **23**, 112–122 (2021).
[32] J. G. Reynolds, T. R. Graham, and C. I. Pearce, J. Mol. Liq. **360**, 119441 (2022).
[33] E. T. Nienhuis, T. R. Graham, N. L. D'Annunzio, M. I. Kowalska, J. A. LaVerne, T. M. Orlando, J. G. Reynolds, D. M. Camaioni, K. M. Rosso, C. I. Pearce, and E. D. Walter, J. Chem. Phys. **158**, 224503 (2023).
[34] J. Ilavsky and P. R. Jemian, J. Appl. Crystallogr. **42**, 347–353 (2009).
[35] G. Beaucage, J. Appl. Crystallogr. **28**, 717–728 (1995).
[36] G. Beaucage, Phys. Rev. E **70**, 031401 (2004).
[37] G. Beaucage, H. K. Kammler, and S. E. Pratsinis, J. Appl. Crystallogr. **37**, 523–535 (2004).
[38] B. Hammouda and D. L. Ho, J. Polym. Sci., Part B: Polym. Phys. **45**, 2196–2200 (2007).
[39] A. M. Smith, A. A. Lee, and S. Perkin, J. Phys. Chem. Lett. **7**, 2157–2163 (2016).
[40] A. A. Lee, C. S. Perez-Martinez, A. M. Smith, and S. Perkin, Phys. Rev. Lett. **119**, 026002 (2017).
[41] M. A. Gebbie, A. M. Smith, H. A. Dobbs, A. A. Lee, G. G. Warr, X. Banquy, M. Valtiner, M. W. Rutland, J. N. Israelachvili, S. Perkin, and R. Atkin, Chem. Commun. **53**, 1214–1224 (2017).
[42] G. Liu, D. Parsons, and V. S. J. Craig, J. Colloid Interface Sci. **579**, 369–378 (2020).
[43] M. Dinpajooh, E. Biasin, E. T. Nienhuis, S. T. Mergelsberg, C. J. Benmore, G. K. Schenter, J. L. Fulton, S. M. Kathmann, and C. J. Mundy, J. Chem. Phys. **161**, 151102 (2024).
[44] G. L. Troyer, M. A. Purcell, and W. I. Winters, J. Radioanal. Nucl. Chem. **263**, 587–592 (2005).
[45] D. E. Irish and M. H. Brooker, Trans. Faraday Soc. **67**, 1916–1922 (1971).
[46] D. E. Irish and R. V. Thorpe, Can. J. Chem. **53**, 1414–1423 (1975).
[47] M. H. Brooker and B. S. deYoung, J. Inorg. Nucl. Chem. **42**, 1217–1221 (1980).
[48] M. H. Brooker and D. E. Irish, Can. J. Chem. **49**, 1289–1295 (1971).
[49] M. U. Belyi, G. I. Gaididei, V. P. Sakun, and M. G. Skryshevskaya, J. Appl. Spectrosc. **62**, 76–82 (1995).
[50] V. Mäemets and I. Koppel, J. Chem. Soc., Faraday Trans. **93**, 1539–1542 (1997).
[51] V. Mäemets and I. Koppel, J. Chem. Soc., Faraday Trans. **94**, 3261–3269 (1998).
[52] J. F. Hinton and E. S. Amis, Chem. Rev. **71**, 627–674 (1971).
[53] J. Davies, S. Ormondroyd, and M. C. R. Symons, Trans. Faraday Soc. **67**, 3465 (1971).